Available online at www.sciencedirect.com
ScienceDirect
Diamond & Related Materials 16 (2007) 550–557
DIAMOND AND RELATED MATERIALS
www.elsevier.com/locate/diamond

Behavior of human umbilical vein endothelial cells on micro-patterned amorphous hydrogenated carbon films produced by plasma immersion ion implantation & deposition and plasma etching

F.J. Jing [a,b], N. Huang [b], L. Wang [b], R.K.Y. Fu [a], Y.F. Mei [a], Y.X. Leng [a,b], J.Y. Chen [b], X.Y. Liu [a,c], Paul K. Chu [a,*]

[a] Department of Physics and Materials Science, City University of Hong Kong, Tat Chee Avenue, Kowloon, Hong Kong, China
[b] Department of Materials Engineering, Southwest Jiaotong University, Chengdu 610031, China
[c] Shanghai Institute of Ceramics, Chinese Academy of Science, 1295 Dingxi Road, Shanghai, 200050, China

Received 24 June 2006; received in revised form 20 September 2006; accepted 13 November 2006
Available online 18 December 2006

Abstract

Amorphous hydrogenated carbon films synthesized by plasma immersion ion implantation and deposition (PIII&D) were micro-patterned using argon plasma etching. Wells containing organized arrays of square holes were produced by plasma etching for 40 min on the surface of the a-C:H films covered by a steel stainless mask. The characteristics of the micro-patterned surfaces including the chemical composition, structure, surface morphology, contact angle, and surface energy were investigated and the effects of surface micro-patterning on the behavior of cultured human umbilical vein endothelial (HUVE) cells were investigated. All the micro-patterned samples exhibit a more hydrophobic nature and both cell adhesion and proliferation on the micro-patterned samples are improved compared to the un-patterned hydrogenated carbon film. The micro-patterns on the hydrogenated carbon films are observed to influence the water contact angle, surface energy, and HUVE cell behaviors, and the surface energy and hydrophobic surfaces appear to be the predominant reasons for the better cell adhesion and more rapid proliferation. Our results demonstrate the feasibility of using micro-patterning to modulate HUVE cell behavior.

PACS: 52.77.Dq; 81.65.cf; 87.68.+z; 87.17.−d
Keywords: Hydrogenated amorphous carbon films; Micro-patterning; Endothelial cell

1. Introduction

Amorphous hydrogenated carbon is a potential material in biomedical devices because of its chemical inertness, low coefficient of friction, high wear resistance, and good biocompatibility. Surface-induced thrombogenesis is known to be one of the reasons for failure of artificial cardiovascular prostheses and stenosis is reduced only when the surface has a layer of viable endothelial cells. Endothelialization of the prosthetic surface is thus a favorable step to mitigate the risk of restenosis and attain better hemocompatibility [1,2]. However, the cell behavior must be investigated in order to better understand the multiple cell–material interactions. Several studies have demonstrated that the surface properties of biomaterials affect the cell behavior including cell attachment, cell proliferation, and cell differentiation [3–5].

The surface topography is generally believed to play an important role in the cell orientation and biocompatibility since Harrison first observed that cells grew on a spider web following the fibers [6]. The surface topography such as micro- and nano-metric patterns can impact the adhesion, motion, spreading, and growth of cells on the surface [7]. Studies of the interactions between the substrate and cells have encompassed many cell types and substratum features including grooves, ridges, steps, pores, wells, nodes, and adsorbed protein

* Corresponding author. Tel.: +86 852 27887724; fax: +86 852 27889549.
E-mail address: paul.chu@cityu.edu.hk (P.K. Chu).

0925-9635/$ - see front matter © 2006 Elsevier B.V. All rights reserved.
doi:10.1016/j.diamond.2006.11.051

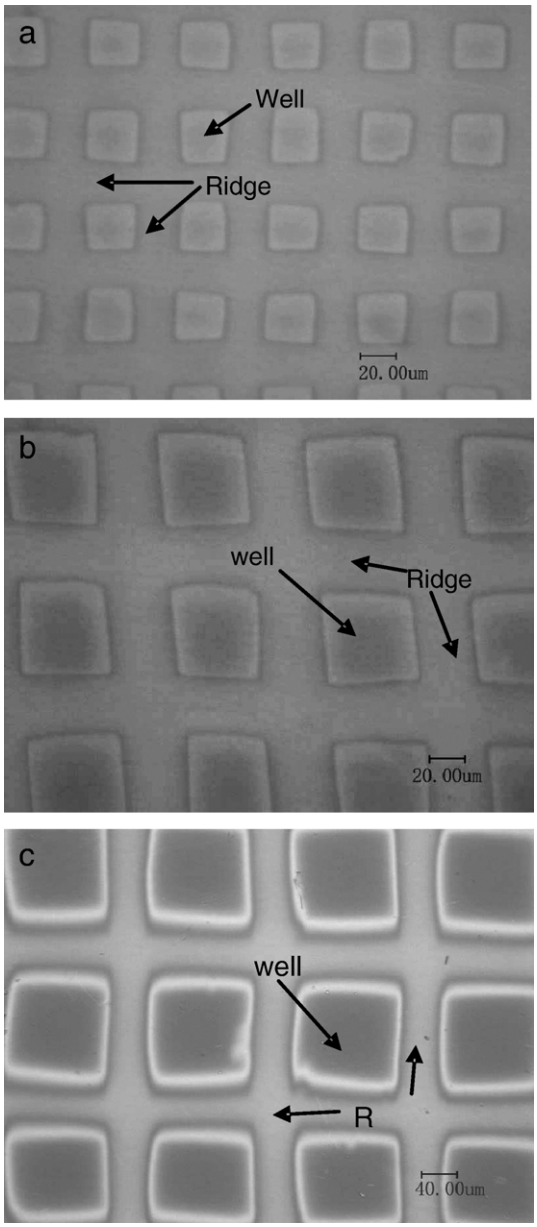

Fig. 1. Optical micrographs of (a) C25, (b) C50, and (c) C100.

fibers. The techniques used to produce features of controlled dimensions include photolithography and reactive ion etching, cutting with diamond or tungsten, laser modification, glancing angle deposition, laser ablation, laser deposition, replica molding of X-ray lithography masters, imprint lithography, micro-contact printing and etching, and ink-jet printing.

In this study, amorphous hydrogenated carbon films were synthesized by plasma immersion ion implantation and deposition (PIII&D) [8], a technique that is suitable for medical devices with complex geometry due to its non-line-of-sight nature. By using an overlying stainless steel mesh, we subsequently patterned the surfaces using argon plasma etching. This method is simpler than most of the patterning techniques reported in the literature. The adhesion and proliferation of behavior of HUVE cells on these micro-patterned surfaces were evaluated.

2. Materials and experimental methods

2.1. Synthesis and micro-patterning of amorphous hydrogenated carbon films

Carbon films were synthesized on (100) silicon wafers using plasma immersion ion implantation and deposition (PIII&D). The substrate initially underwent argon plasma cleaning for 15 min at a pressure of about 5.7×10^{-2} Pa using a radio frequency (RF) power of 500 W and substrate DC bias of 600 V. Afterwards, acetylene and argon were bled into the vacuum chamber at flow rates of 20 and 5 sccm (standard cubic centimeters per minute), respectively, and the mixed acetylene and argon plasma was produced using an RF power of 500 W. Negative voltage pulses of 20 kV with a width of 400 μs and repetition rate of 40 Hz were applied to the substrate to conduct PIII&D and the processing time was 3 h.

In our experiments, plasma ion etching was employed to control the etching depths. As shown in Fig. 1, stainless steel masks with square holes of dimensions of 25 μm × 25 μm (used on sample C25), 50 μm × 50 μm (used on sample C50), and 100 μm × 100 μm (used on sample C100) covered the surface of the amorphous hydrogenated carbon films that were biased to −600 V DC during plasma etching. During etching, the argon flow rate was 30 sccm and etching time was 40 min. The structure of the as-deposited and micro-patterned amorphous hydrogenated carbon films was determined by a Renishaw RM3000 Micro-Raman system with a beam size of 5 μm. Fourier transform infrared spectroscopy (FTIR) conducted on a NICOLET 5700 was employed to investigate the chemical bonds in the films. The chemical composition and bonding states of the films were determined by XPS with an energy resolution of 0.9 eV using a Mg anode without a monochromator. The film thickness and line scans were measured using an AMBIOS XP-2 surface profiler.

2.2. Surface energy measurements

The surface wettability and tension of the deposited amorphous hydrogenated carbon films were determined using a RAME-HART contact angle goniometer. The size of the sessile drop is about 2–3 mm in diameter. The surface energy (γ_s), Lifshitz–van der Waals interactions (γ_s^{LW}), acid–base interactions (γ_s^{AB}), basic component (γ_s^-), and acid component

Table 1
Surface energy parameters of test liquids (mJ/m^2)

Samples	γ_l^+	γ_l^-	γ_l^{AB}	γ_l^{LW}	γ_l
Water	25.5	25.5	51.0	21.8	72.8
Glycerol	3.9	57.4	30.0	34.0	64.0
Diiodomethane	0	0	0	50.8	50.8
Formamide	2.3	39.6	19.0	39.0	58.0

(γ_s^+) were calculated by the van Oss technique [9]. For a non-polar liquid,

$$\gamma_s^{LW} = \frac{\gamma_l^{LW}(1+\cos\theta)^2}{4}. \quad (1)$$

For polar liquids, the values of (γ_s^+) and (γ_s^-) can be derived from linear fitted curves using Eq. (2). The values of (γ_s^{AB}) and (γ_s) can be determined using Eqs. (3) and (4) respectively:

$$\frac{\gamma_l(1+\cos\theta)-(\gamma_s^{LW})^{1/2}(\gamma_l^{LW})^{1/2}}{2(\gamma_l^-)^{1/2}} = (\gamma_s^+)^{1/2} + \frac{(\gamma_l^+)^{1/2}}{(\gamma_l^-)^{1/2}}(\gamma_s^-)^{1/2}, \quad (2)$$

$$\gamma_s^{AB} = 2(\gamma_s^+)^{1/2}(\gamma_s^-)^{1/2}, \quad (3)$$

$$\gamma_s = \gamma_s^{LW} + \gamma_s^{AB}. \quad (4)$$

Here, θ is the contact angle and γ_l, γ_l^{LW}, γ_l^{AB}, γ_l^- and γ_l^+ are the liquid phase parameters. Three polar (water, glycerin and formamide) liquids and one non-polar liquid (diiodomethane) were used in the measurements and the surface free energy parameters of these liquids are shown in Table 1 [10].

2.3. HUVE cell cultures

Human umbilical vein endothelial cells (HUVEC) were isolated and cultured according to the method of Jaffe et al. [11]. The umbilical cord was first washed thoroughly and the blood in the umbilical vein was drained. The vein was then incubated with 0.1% type II collagenase in medium 199 for 10 min at 37 °C to detach the endothelial cells. The lumen of the vein was rinsed 3 times using serum-free medium 199. All the digestive and rinsing liquids were collected and centrifuged at 1000 rpm for 5 min. After the supernatant liquid was discarded, it was diluted with complete medium 199 and blended sufficiently to obtain the cell incubation liquid. The samples were sterilized by autoclaving at 120 °C for 1 h and then placed in the 48-well culture plate. Then 200 μl drops of the incubation liquid cell were added onto the samples. All the samples were incubated at 37 °C in 5% CO_2/air for 1–3 days. The complete medium contained M199 powders (9.5 g/l), 20% newborn calf serum, 2 mM L-glutamine, 20 mM *N*-2-hydroxyethylpiperazine-*N*-2-ethanesulfonic acid (HEPES), 20 μg/ml endothelial cell growth factor (ECGF), penicillin (100 U/ml), streptomycin sulfate (100 μg/ml), pyruvic acid sodium (0.11 g/l), and sodium bicarbonate (2.2 g/l). These samples were subsequently rinsed thrice with a phosphate buffered solution (PBS) solution to remove weakly adherent endothelial cells. The adhered endothelial cells (EC) were fixed in 2% and 5% glutaraldehyde in the PBS solution at room temperature for 2 and 12 h, respectively, followed by dehydrating and critical point drying. The dried cells were then sputter-coated with gold before examination by optical microscopy and scanning electron microscopy. Ten fields at a magnification factor of 200 were chosen at random to obtain statistical quantity averages of the adherent cells based on the point counting method.

3. Results

3.1. Characteristics of the deposited and micro-patterned amorphous hydrogenated carbon films

The surface topography of the micro-patterned carbon films observed by optical microphotography is shown in Fig. 1. Fig. 2 shows the line scans of samples C25, C50, C100, and the as-deposited carbon film obtained by surface profilometry. The position of the well and ridge can be confirmed in the surface line scans and optical photographs obtained by surface profilometry. The surface of the as-deposited carbon film is relatively smooth and the film thickness is about 300 nm. As shown in Fig. 1, the mean well width and ridge width are about 25 μm and 25 μm for sample C25 and these values are very similar to the mask

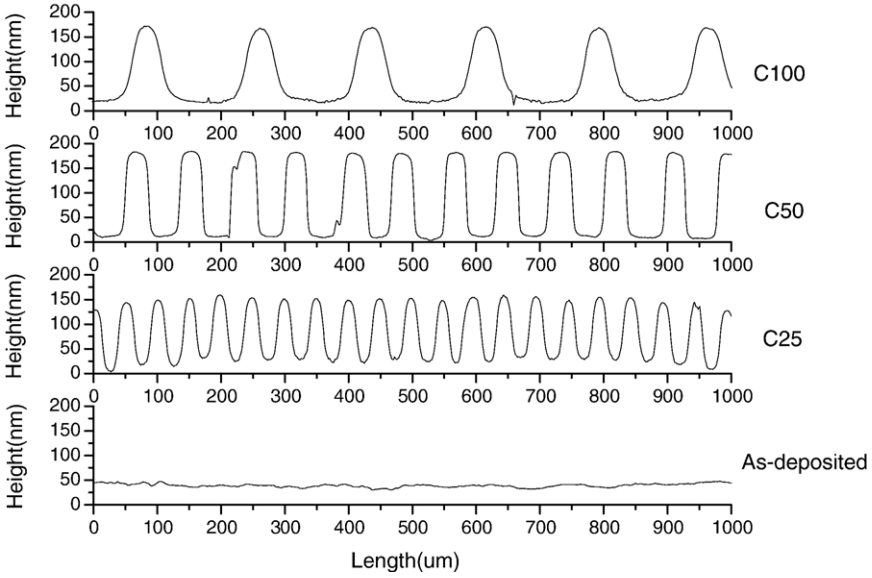

Fig. 2. Surface line scans acquired from as-deposited carbon film, C25, C50, and C100.

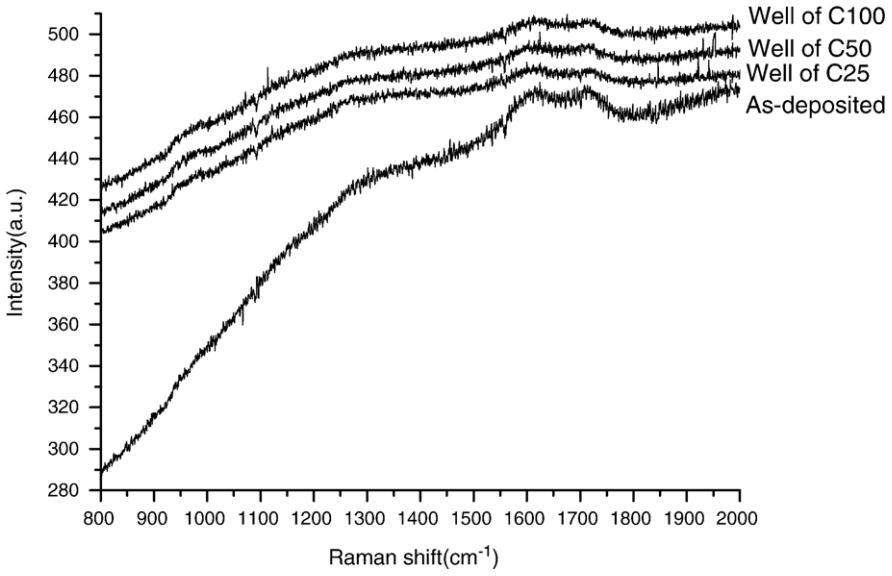

Fig. 3. Raman spectra acquired from the as-deposited carbon film and wells of samples C25, C50, and C100.

dimensions. The mean well and ridge widths are about 55 μm and 40 μm for sample C50, showing a small increase in the width but a decrease in the ridge compared to the mask dimensions. In comparison, the mean well and ridge widths are about 120 μm and 60 μm for sample C100, respectively revealing a significant increase in the well width and decrease in the ridge width. The widths of the ridges in comparison with the mask dimensions were evaluated from the FWHMs of the peaks based on the line scans in Fig. 2 and optical photos obtained by surface profilometry. As shown in Fig. 2, the depths of the square wells are about 150 nm for samples C25, C50 and C100 and the as-deposited carbon film is relatively smooth. Our results show that argon etching produces more isotropic square wells with bigger masks, that is, more undercutting underneath the mask.

Fig. 3 shows the micro-Raman spectra around the excitation wavelength of 514.5 nm acquired using a 5 micrometer beam size from the as-deposited carbon films and wells of samples C25, C50 and C100. The micro-Raman spectrum of the as-deposited carbon film shows two broad peaks at 1300–1450 cm^{-1} and 1500–1650 cm^{-1} as shown in Fig. 3. Such a spectrum with an asymmetric broad peak is often seen in deposited carbon films. The features at 950 cm^{-1} are the second order Raman peaks originating from the Si substrate. All the samples show a high photoluminescence background intensity that is indicative of a polymer-like constituent in the as-deposited carbon films and etched wells of C25, C50, and C100 [12]. The variation in the photoluminescence (PL) observed here is similar to that observed by Rusli et al. [13] in a-C/H

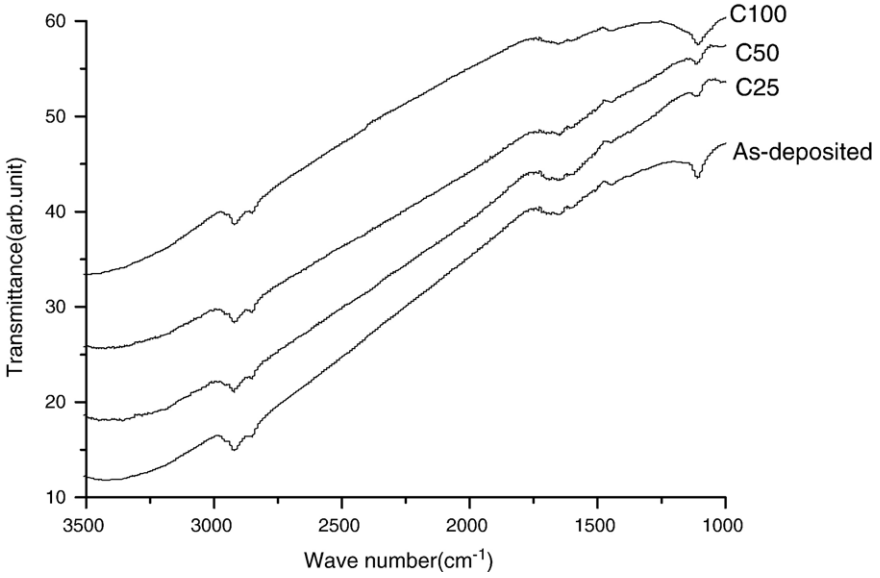

Fig. 4. FTIR spectra acquired from the control and samples C25, C50, and C100.

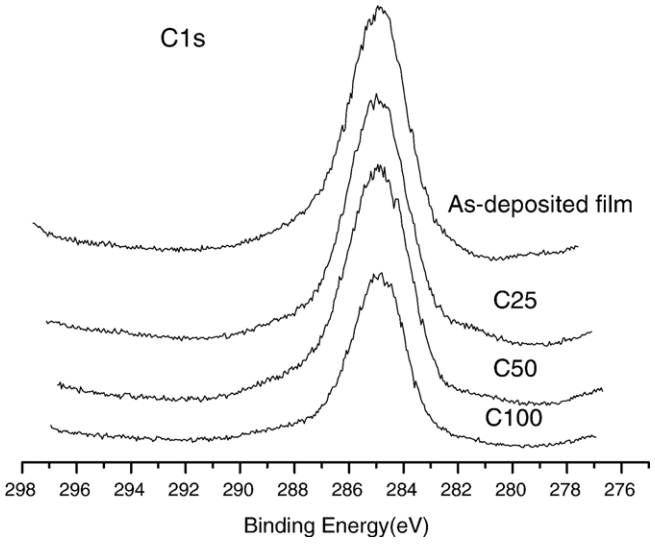

Fig. 5. XPS C1s spectra obtained from the control and samples C25, C50, and C100.

films. It is proposed that this photoluminescence arises from radiative recombination of the electron-hole pairs confined to the π states of the sp^2 bonded clusters in a sp^3 bonded amorphous matrix.

FTIR can more easily discern C–H sp^2 and sp^3 bonds. Fig. 4 shows the FTIR spectra of the as-deposited carbon film, C25, C50, and C100. The features at 1100 cm^{-1} arise from SiO_2 present in the silicon wafer before deposition. The C–H bending mode is observed at 1450 cm^{-1} due to sp^3 CH_2 (asymmetrical). The features at 2850 cm^{-1} are due to sp^3 CH_2 (symmetrical) and that at 2920 cm^{-1} derives from sp^3 CH_2 (asymmetrical). In addition, a peak at 1700 cm^{-1} is attributed to the C═C stretching vibration [14]. These peaks are observed in the as-deposited carbon film as well as samples C25, C50 and C100. The IR results reveal that hydrogen atoms are essentially bonded to the amorphous carbon skeleton in the form of sp^3 C–H bonds in all the samples. It is consistent with other reported results that hydrogen in a polymer-like C:H film is mainly in the sp^3 C–H groups with a large oscillator strength compared to hydrogen in a hard C:H film which is mainly in the sp^2 C–H groups with a smaller oscillator strength [15].

Fig. 5 exhibits the XPS C1s spectra of the as-deposited carbon film, C25, C50, and C100 samples. It is known that the C1s peak of graphite (sp^2) is at 284.0–284.5 eV, 285.0–285.2 eV for diamond (sp^3), 284.9–285.5 eV for C–H, and 286.4–290 eV for C–O and C═O [16]. The corresponding C1s spectra can be deconvoluted into three peaks situated at approximately 284.3, 285.1 and 287 eV. Our results show that C1s spectra do not vary significantly among the as-deposited carbon film, C25, C50, and C100.

Table 2
Contact angles (degrees) on as-deposited and micro-patterned carbon films using four different test liquids

Sample	Water	Diiodomethane	Glycerin	Formamide
As-deposited	62.5±3.5	30.5±0.8	35.9±1.5	16.2±2.3
C25	114.5±2.2	24.5±3.0	78.9±1.7	68.5±1.5
C50	117.8±1.4	23.0±2.3	84.5±5.5	62.4±2.5
C100	120.6±2.4	19.4±1.4	108.4±2.1	36.5±3.8

Table 3
Mean surface energy components (mJ/m^2) of the as-deposited and micro-patterned carbon films

Samples	γ_s^+	γ_s^-	γ_s^{AB}	γ_s^{LW}	γ_s
As-deposited	1.77	14.95	10.29	44.01	54.31
C25	0.02	4.58	0.59	46.33	46.92
C50	0.09	4.19	1.22	46.84	48.07
C100	0.11	8.88	1.98	47.96	49.94

3.2. Surface energy

Table 2 lists the contact angles of water, diiodomethane, glycerol and formamide on the as-deposited film, C25, C50, and C100. The micro-patterned samples have larger contact angles with polar liquids compared to the control, whereas the contact angles with the non-polar liquid diiodomethane decrease relative to the as-deposited carbon film. Using the van Oss technique, the mean surface free energy parameters are calculated and tabulated in Table 3. The acid–base interactions (γ_s^{AB}), basic component (γ_s^-), acid component (γ_s^+) of samples C25, C50 and C100 decrease and the Lifshitz–van der Waals interactions (γ_s^{LW}) increase slightly in comparison with those of the control. The results show that the micro-patterned surfaces are more hydrophobic than the as-deposited film.

3.3. HUVE cell cultures

Fig. 6 displays the statistical results of the number of HUVE cells adhered on the surface of the as-deposited and micro-patterned carbon films. The cell numbers on samples C25, C50 and C100 increase compared to the as-deposited films after the first and third days. The surface morphology of typical endothelial cells is exhibited in Fig. 7. The cells show a rough

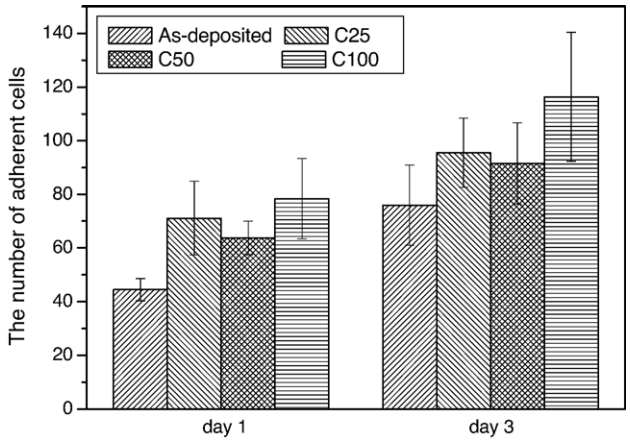

Fig. 6. Statistical results of the number of HUVE cells adhering onto the surfaces of the as-deposited carbon film, C25, C50, and C100 after 1 and 3 days of cell culturing.

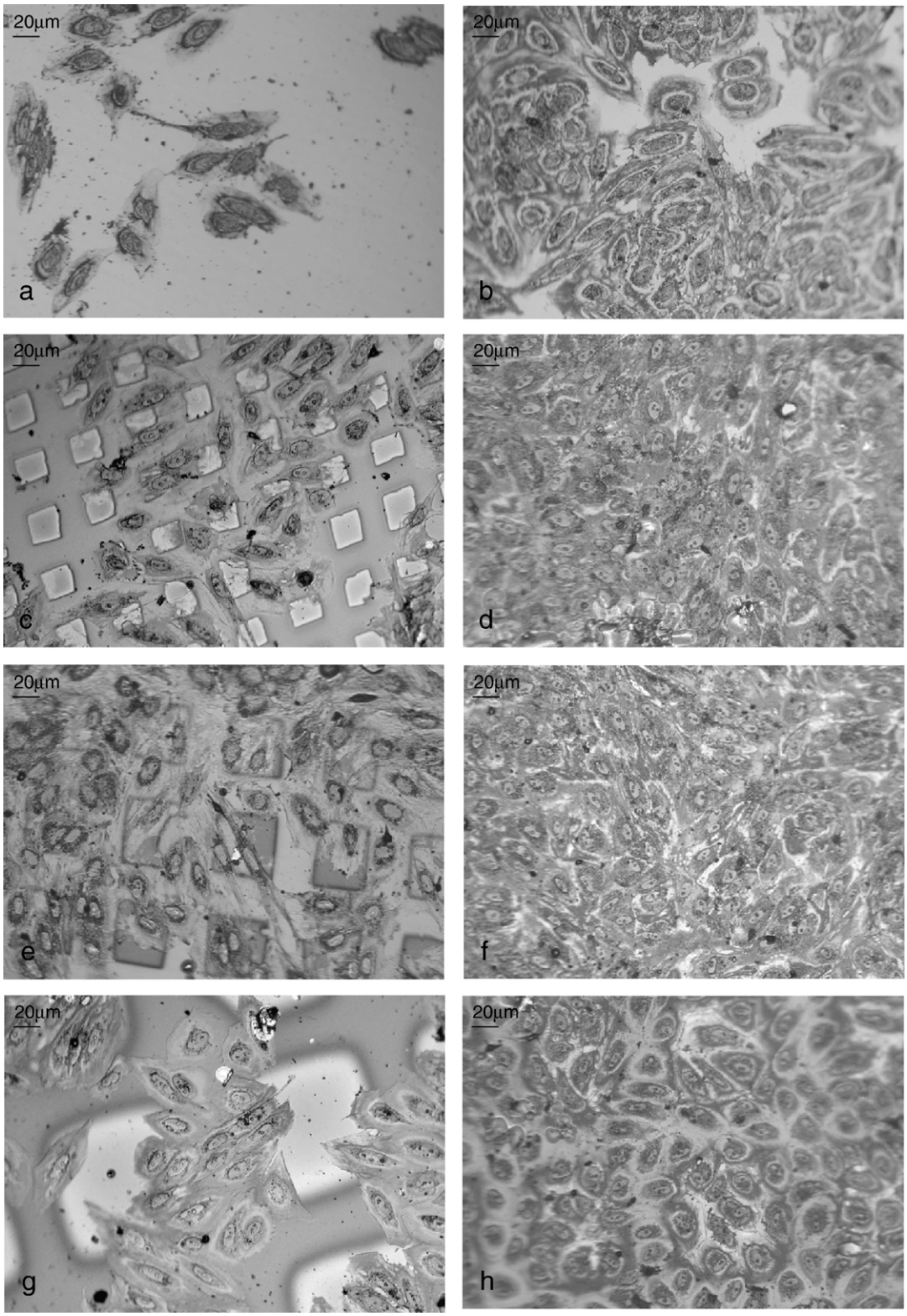

Fig. 7. Optical micrographs showing the proliferation of the HUVE cells after 1 and 3 days of culturing: (a) as-deposited carbon films after 1 day, (b) as-deposited carbon films after 3 days; (c) sample C25 after 1 day, (d) sample C25 after 3 days, (e) sample C50 after 1 day, (f) sample C50 after 3 days, (g) sample C100 after 1 day, and (h) C100 after 3 days.

inclination of adhering onto the ridges of the micro-patterned samples but cell alignment cannot be clearly identified. After 3 days, the HUVE cells grow to a confluent monolayer with a cobblestone-like EC morphology. The morphology of the wells and ridges on C25, C50 and C100 can no longer be observed due to extensive cell proliferation covering the surface. Our

results show that the HUVE cells adhere and proliferate well on the wells of samples C25, C50 and C100. Both cell adhesion and proliferation are observed to be enhanced on the micro-patterned samples compared to the as-deposited DLC.

4. Discussion

Amorphous hydrogenated carbon films prepared by PIII&D show good cytocompatibility based on the HUVE cell culturing results. The hydrogenated carbon films containing carbon and hydrogen are biologically compatible. FTIR and XPS results show that argon plasma sputtering does not affect significantly the chemical nature of the hydrogenated carbon films. Micro-Raman results show that argon sputtering only reduces the peak intensity. Therefore, the surface energy and endothelial cell behavior appear to be influenced more by the topography of the micro-patterns.

Some mechanisms have been proposed to explain the cell-surface adhesion from the macroscopic and atomic viewpoints [17]. The macroscopic model proposes that cell adhesion depends upon physiochemical properties of the surfaces, charges, and hydrophobicity [18], whereas the atomic model argues that adhesion is basically due to receptor–ligand type interactions. It has also been reported that some physical properties of the surfaces including the surface energy, porosity, and roughness of the surface can enhance endothelialization on biomaterials [19–23]. Our observations indeed show that the micro-patterns on the carbon films influence the local contact angles, surface energy, and HUVE cell behavior. All the micro-patterned samples have larger contact angles with the test liquids than the as-deposited control. The hydrophobicity of the micro-patterned surface is believed to be caused by the surface topography generated by plasma etching. The changes in the wettability observed in our experiments are somewhat different from those in few other reports that surface roughness improves wetting in hydrophilic situations and degrades it in hydrophobic ones [24]. However, our observations are consistent with those of Herminghaus [25] who has suggested that if the contact angle is smaller than 90°, the liquid can span the indentations and increase the macroscopic contact angle. The difference observed for diiodomethane may be due to the different air pockets inside the wells changing the contact angle. The existence of air pockets on a crenellated surface has in fact been observed to modify the contact angle by J. Bico [24].

Van der Waals and hydrophobic forces appear to be the more important parameters affecting cell adhesion. A direct correlation exists between the electron-donor component of the surface free energy and adhesion of the HUVE cells. The number of adhered cells increases with a decreasing electron-donor component of the surface free energy. The hydrophobic surfaces can induce irreversible adsorption of high-molecular-weight proteins such as fibronectin [26] and fibrinogen [27]. Fibronectin is synthesized by the endothelial cells and present in the extracellular matrix playing an important role in the adhesion process of mammalian cells through specific interactions with cellular membrane receptors. This binding activates a signaling cascade of cell migration, proliferation, or differentiation resulting in higher cell adhesion and proliferation with higher surface energy on some of the micro-patterned surfaces. Such different responses of the HUVE cells to the surface topography observed here may be related to these factors.

5. Conclusion

Hydrogenated amorphous carbon films were fabricated by plasma immersion ion implantation and deposition and subsequently micro-patterned by argon plasma etching. The micro-patterned surfaces show organized arrays of square wells. Argon plasma sputtering exerts a small influence on the chemical structure of the hydrogenated carbon films. The micro-patterns on the carbon films change the contact angles, surface energies, and HUVE cell behavior. Both cell adhesion and proliferation of HUVE cells are enhanced on the micro-patterned samples and the surface energy and hydrophobic surfaces are believed to play important roles in the cell adhesion. Our results demonstrate that surface micro-patterning using plasma etching alters the HUVE cell behavior on hydrogenated carbon films.

Acknowledgments

This work was financially supported by Hong Kong Research Grants Council (RGC) and National Science Foundation of China (NSFC) Joint Research Scheme No. N_CityU 101/03.

References

[1] B.L. Seal, T.C. Otero, A. Panitch, Mater. Sci. Eng. 34 (2001) 147.
[2] Y.B. Zhu, C.Y. Gao, T. He, J.C. Shen, Biomaterials 25 (2004) 423.
[3] A. Naji, M.F. Harmand, J. Biomed. Mater. Res. 24 (1990) 861.
[4] U. Meyer, D.H. Saulczewsi, K. Moller, H. Heide, D.B. Jones, Cells Mater. 3 (1993) 129.
[5] J.G. Steele, C.D. Mcfarland, B.A. Dalton, G. Hohnson, M.D.M. Evans, C.R. Howlett, P.A. Underwood, J. Biomaterials Sci., Polym. Ed. 5 (1993) 245.
[6] R.G. Harrison, Science 34 (1911) 279.
[7] R.G. Flemming, C.J. Murphy, G.A. Abrams, S.L. Goodman, P.F. Nealey, Biomaterials 20 (1999) 573.
[8] P.K. Chu, S. Qin, C. Chan, N.W. Cheung, L.A. Larson, Mater. Sci. Eng., R Rep. 17 (6–7) (1996) 207.
[9] C.J. van Oss, Interfacial Forces in Aqueous Media, Marcel Dekker, New York, 1994.
[10] J. Azeredo, I. Ramos, L. Rodrigues, R. Oliveira, J. Teixeira, J. Inst. Brew. 103 (1997) 359.
[11] E.A. Jaffe, R.L. Nachman, C.G. Becker, C.R. Minick, J. Clin. Invest. 52 (1973) 2745.
[12] M. Yoshikawa, G. Katagiri, H. Ishida, A. Ishitani, T. Akamatsu, J. Appl. Phys. 64 (1988) 6464.
[13] J. Rusli, J. Robertson, G.A.J. Amaratunga, J. Appl. Phys. 80 (1996) 2998.
[14] J. Robertson, Mater. Sci. Eng., R Rep. 37 (2002) 129.
[15] A. von Keudell, Thin Solid Films 402 (2002) 1.
[16] P. Yang, N. Huang, Y.X. Leng, J.Y. Chen, R.K.Y. Fu, S.C.H. Kwok, Y. Leng, P.K. Chu, Biomaterials 24 (2003) 2821.
[17] B.W. Metcalf, B.J. Dalton, Cellular Adhesion, Plenum Press, New York, 1994.
[18] A. Harris, Exp. Cell Res. 77 (1973) 285.
[19] M.L. Warocquier, R. Clerout, C. Legris, M. Degrange, M.F. SigotLuizard, J. Biomed. Mater. Res. 36 (1997) 99.

[20] K. Kieswetter, Z. Schwartz, T.W. Hummert, D.L. Cocharn, J. Simpson, D.D. Dean, B.D. Boyan, J. Biomed. Mater. Res. 32 (1996) 55.
[21] J.Y. Martin, Z. Schwartz, T.W. Hummert, D.L. Schraub, J. Simpson, J. Lankford, D.D. Dean, D.L. Cocharn, B.D. Boyan, J. Biomed. Mater. Res. 29 (1995) 389.
[22] S.V. Madihally, H.W.T. Matthew, Biomaterials 20 (1999) 1133.
[23] A.K. Salem, R. Stevens, R.G. Pearson, M.C. Davies, S.J.B. Tendler, C.J. Roberts, P.M. Williams, K.M. Shakesheff, J. Biomed. Mater. Res. 61 (2002) 212.
[24] J. Bico, C. Marzolin, D. Quere, Europhys. Lett. 47 (2) (1999) 220.
[25] S. Herminghaus, Europhys. Lett. 52 (2000) 165.
[26] D.R. Absolom, W. Zingg, A.W. Neumann, J. Biomed. Mater. Res. 21 (1987) 161.
[27] G. Altankov, T. Groth, J. Mater. Sci. 5 (1994) 732.